

Charged Higgs production at linear colliders in large extra dimensions

Qiang Li^{a*}, Chong Sheng Li^a †, Robert J. Oakes^{b‡}, and Li Lin Yang^{a§}

^a *Department of Physics, Peking University, Beijing 100871, China*

^b *Department of Physics and Astronomy,
Northwestern University, Evanston, IL 60208-3112, USA*

(Dated: May 3, 2019)

Abstract

In the Two-Higgs-Doublet Model(2HDM) with large extra dimensions(LED), we study the contributions of virtual Kaluza-Klein(KK) gravitons to 2HDM charged Higgs production, especially in the two important production processes $e^+e^- \rightarrow H^+H^-$ and $e^+e^- \rightarrow H^-t\bar{b}$, at future linear colliders (LC). We find that KK graviton effects can significantly modify these total cross sections and also their differential cross sections compared to their respective 2HDM values and, therefore, can be used to probe the effective scale Λ_T up to several TeV. For example, at $\sqrt{s} = 2$ TeV, the cross sections for $e^+e^- \rightarrow H^+H^-$ and $e^+e^- \rightarrow H^-t\bar{b}$ in the 2HDM are 7.4fb for $m_{H^-} = 150$ GeV and 0.003fb for $m_{H^-} = 1.1$ TeV and $\tan\beta = 40$, while in LED they are 12.1fb and 0.01fb, respectively, for $\Lambda_T = 4$ Tev.

PACS numbers: 11.10.Kk, 12.60.Jv, 14.80.Cp

* Electronics address: qliphy@pku.edu.cn

† Electronics address: csli@pku.edu.cn

‡ Electronics address: r-oakes@northwestern.edu

§ Electronics address: llyang@pku.edu.cn

I. INTRODUCTION

The idea that quantum gravity can appear at the TeV energy scale well below the Planck mass $M_p \sim 1.2 \times 10^{19} \text{ GeV}$ was proposed in the 1990's[1, 2, 3, 4, 5, 6]. The large extra dimensions(LED) model[1] introduced by Arkani-Hamed, Dimopoulos and Davli has attracted much attention. It has been emphasized that the presence of large extra dimensions brings a new solution to the hierarchy problem, which can take the place of other mechanisms, for example, low-energy supersymmetry. However, it is also interesting to examine a scenario which combines new physics beyond the Standard Model(SM) such as the 2HDM[7] and LED. This new possibility leads to different phenomenology than the usual LED scenario, which we explore here.

In this extended LED scenario, as in the usual LED scheme, the total space-time has $D = 4 + \delta$ dimensions. The SM and new particles beyond the SM live in the usual $3 + 1$ -dimensional space, while gravity can propagate in the additional δ -dimensional space, which is assumed for simplicity to be compactified on the δ -dimensional torus T^δ with a common radius R . Then the 4-dimensional Planck scale M_p is no longer the relevant scale but is related to the fundamental scale M_s as follows[1, 8]:

$$M_p^2 = M_s^{\delta+2} (2\pi R)^\delta, \quad (1)$$

where $M_s \sim \text{TeV}$. According to Eq. (1), deviations from the usual Newtonian gravitational force law can be expected at distances smaller than $R \sim 2.10^{-17} 10^{\frac{32}{\delta}} \text{ cm}$ [8]. For $\delta \geq 2$, LED is consistent with the current experiments[9] since gravitational forces are not yet well probed at distances less than about a millimeter (However for $\delta = 2$, there are constraints arising from, e.g., supernova cooling, which require $M_s \geq 10 - 100 \text{ TeV}$ if $\delta = 2$ [8]).

2HDM LED can be tested at future high energy colliders. In 2HDM LED, just as in LED, there exist KK towers of massive spin-2 gravitons and scalars which can interact with the SM and beyond SM fields. There are two classes of effects that can probe LED: real graviton emission and virtual KK tower exchange.

At future linear colliders the search for one or more Higgs bosons will be a central task. In the SM, the Higgs boson mass is a free parameter with an upper bound of $m_H \leq 600 - 800 \text{ GeV}$ [10]. Beyond the SM, the 2HDM is of particular theoretical interest, in which the two complex Higgs doublets correspond to eight scalar states and spontaneous symmetry

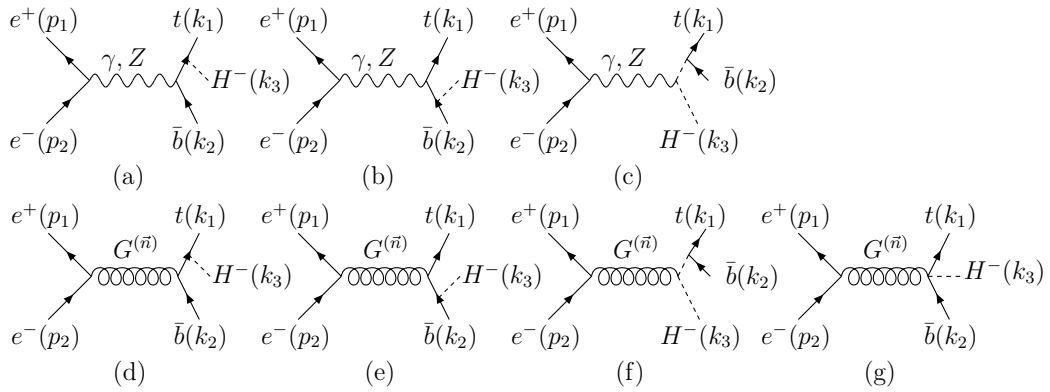
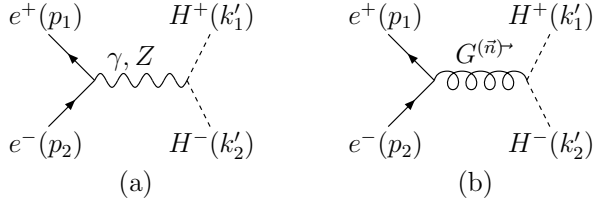
breaking leads to five physical Higgs bosons: two neutral CP-even bosons h^0 and H^0 , one neutral CP-odd boson A^0 , and two charged bosons H^\pm . The h^0 is the lightest and is a SM-like Higgs boson especially in the decoupling region ($m_{A^0} \gg m_{Z^0}$). The other four are not SM-like and their discovery, particularly the charged Higgs bosons, would provide evidence for the 2HDM. If the H^\pm bosons have mass $m_{H^\pm} < m_t - m_b$, they will be produced mainly through the $t \rightarrow bH^+$ decays of top quarks, which can be produced singly or in pairs at an e^+e^- LC [11]. If there is sufficient center of mass energy available, $\sqrt{s} > 2m_{H^\pm}$, then charged Higgs pair production, $e^+e^- \rightarrow H^+H^-$, will be the dominant production mechanism[11]. However, if $m_{H^\pm} > \max(m_t - m_b, \sqrt{s}/2)$, then H^\pm bosons can only be produced singly. And $e^+e^- \rightarrow H^-t\bar{b}$ [12, 13] is one of the most important single charged Higgs production processes that can also be used to measure the relevant Yukawa couplings. Therefore, for this process, we will focus on the regime where $\sqrt{s}/2 < m_{H^\pm} < \sqrt{s} - m_t - m_b$. For $\sqrt{s} = 500$ GeV (1000 GeV), this implies that $250 < m_{H^\pm} < 320$ GeV ($500 < m_{H^\pm} < 820$ GeV).

There are several kinds of such 2HDM models. In the model called type I, one Higgs doublet provides masses for both the up-type and down-type quarks. In the type II model, one Higgs doublet gives masses to the up-type quarks and the other one to the down-type quarks. In the type III model, both doublets contribute to generate the masses for up-type and down-type quarks. In this paper, we will concentrate on the type II 2HDM(2HDM II), which are favored by the Minimal Supersymmetric Standard Model (MSSM)[14]. We will also briefly discussed the results in the type I 2HDM.

In the following we consider the contributions of virtual KK gravitons to the 2HDM charged Higgs production, especially in the two important production processes $e^+e^- \rightarrow H^+H^-$ and $e^+e^- \rightarrow H^-t\bar{b}$ at future linear colliders. The presentation is organized as follows: In Sect. II we present the calculations. In Sect. III we give the numerical results and discuss them. Sec. IV contains a brief conclusion.

II. ANALYTIC CALCULATIONS

In this section we derive the cross section for 2HDM charged Higgs production. The 2HDM diagrams, including the additional virtual KK gravitons($G_{\mu\nu}^{(\vec{n})}$), which contribute to the processes $e^+e^- \rightarrow H^+H^-$ and $e^+e^- \rightarrow H^-t\bar{b}$ are presented in Figs. 1 and 2, respectively.



In the four dimensional description the interaction Lagrangian between the scattering fields and the KK gravitons ($G_{\mu\nu}^{(\vec{n})}$) or KK scalars ($H^{(\vec{n})}$) is given by [15]

$$\mathcal{L}_{int} = -\frac{1}{M_p} \sum_{\vec{n}} \left(G_{\mu\nu}^{(\vec{n})} T^{\mu\nu} - \frac{1}{3} \sqrt{\frac{3(n-1)}{n+2}} H^{(\vec{n})} T_\mu^\mu \right), \quad (2)$$

where $\vec{n} = (n_1, n_2, \dots, n_\delta)$ with n_i 's being integers, $\bar{M}_p = M_p/\sqrt{8\pi} \sim 2.4 \times 10^{18} \text{ GeV}$ is the reduced four dimensional Planck scale, and $T_{\mu\nu}$ is the energy-momentum tensor of the scattering fields. The n -th KK mode graviton and scalar masses squared are both characterized by $m_{(\vec{n})}^2 = |\vec{n}|^2/R^2$. Since the trace of the energy-momentum tensor is proportional to the mass of the fields due to the field equations, we neglect processes mediated by the KK scalars in our study for the linear e^+e^- collider, and consider only the processes mediated by the KK gravitons.

From Eq. (2) we can derive the relevant Feynman rules to be used in our calculations,

which can be found in Ref. [15, 16]. The numerator of the graviton propagator $P^{\mu\nu\alpha\beta}$ in the unitary gauge[15], is given by:

$$P^{\mu\nu\alpha\beta} = \frac{1}{2} \left(\eta^{\mu\alpha}\eta^{\nu\beta} + \eta^{\mu\beta}\eta^{\nu\alpha} - \frac{2}{3}\eta^{\mu\nu}\eta^{\alpha\beta} \right) + \dots, \quad (3)$$

where $\eta^{\mu\nu}$ is the Minkowski metric. The dots represent terms proportional to the graviton momentum q_μ , and since $q^\mu T_{\mu\nu} = 0$, give a vanishing contribution to the amplitude. Note that the the numerator of the graviton propagator in Ref. [16] is twice Eq. (3) and is the same as presented in Ref. [15]. However, the coupling constant squared in Ref. [15], i.e., $(\sqrt{8\pi}/M_p)^2$ in Eq. (2) is twice the one in Ref. [16]. Hence the results in the two references are consistent and we have been careful of this issue in our calculations.

We can write the amplitudes for the Feynman diagrams shown in Figs.1 and 2 as follows:

$$\begin{aligned} \mathcal{M}_{1a} &= \frac{ie^2}{s} \bar{v}(p_1)(\not{k}_2 - \not{k}_1)u(p_2) + \frac{ie^2(c_w^2 - s_w^2)}{2(s - m_z^2)c_w^2s_w^2} \bar{v}(p_1)(\not{k}_2 - \not{k}_1)[(\frac{1}{2} - s_w^2)P_L - s_w^2P_R]u(p_2) \\ \mathcal{M}_{1b} &= \frac{i\mathcal{G}P^{\mu\nu\alpha\beta}}{4} \chi_{\alpha\beta}^a \bar{v}(p_1)C_{\mu\nu}u(p_2) \\ \mathcal{M}_{2a} &= \frac{-ie^2g}{3\sqrt{2}m_w s[(k_1 + k_3)^2 - m_b^2]} \bar{v}(p_1)\gamma_\mu u(p_2)\bar{u}(k_1, m_t) \left[m_b \tan \beta P_R + m_t \cot \beta P_L \right] \\ &\quad (\not{k}_1 + \not{k}_3 + m_b)\gamma^\mu v(k_2, m_b) + \\ &\quad \frac{-ie^2g}{\sqrt{2}m_w(s - m_z^2)c_w^2s_w^2[(k_1 + k_3)^2 - m_b^2]} \bar{v}(p_1)\gamma_\mu[(\frac{1}{2} - s_w^2)P_L - s_w^2P_R]u(p_2).\bar{u}(k_1, m_t) \\ &\quad \left[m_b \tan \beta P_R + m_t \cot \beta P_L \right] (\not{k}_1 + \not{k}_3 + m_b)\gamma^\mu[(\frac{1}{2} - \frac{1}{3}s_w^2)P_L - \frac{1}{3}s_w^2P_R]v(k_2, m_b) \\ \mathcal{M}_{2b} &= \frac{-2ie^2g}{3\sqrt{2}m_w s[(k_2 + k_3)^2 - m_t^2]} \bar{v}(p_1)\gamma_\mu u(p_2)\bar{u}(k_1, m_t)\gamma^\mu(\not{k}_2 + \not{k}_3 - m_t) \\ &\quad \left[m_b \tan \beta P_R + m_t \cot \beta P_L \right] v(k_2, m_b) + \\ &\quad \frac{ie^2g}{\sqrt{2}m_w(s - m_z^2)c_w^2s_w^2[(k_2 + k_3)^2 - m_t^2]} \bar{v}(p_1)\gamma_\mu[(\frac{1}{2} - s_w^2)P_L - s_w^2P_R]u(p_2).\bar{u}(k_1, m_t) \\ &\quad \gamma^\mu[-(\frac{1}{2} - \frac{2}{3}s_w^2)P_L + \frac{2}{3}s_w^2P_R](\not{k}_2 + \not{k}_3 - m_t) \left[m_b \tan \beta P_R + m_t \cot \beta P_L \right] v(k_2, m_b) \\ \mathcal{M}_{2c} &= \frac{-ie^2g}{\sqrt{2}m_w s[(k_1 + k_2)^2 - m_{H^-}^2]} \bar{v}(p_1)(2\not{k}_3 - \not{p}_1 - \not{p}_2)u(p_2) \\ &\quad \bar{u}(k_1, m_t) \left[m_b \tan \beta P_R + m_t \cot \beta P_L \right] v(k_2, m_b) + \\ &\quad \frac{-ie^2g(c_w^2 - s_w^2)}{2\sqrt{2}m_w(s - m_z^2)c_w^2s_w^2[(k_1 + k_2)^2 - m_{H^-}^2]} \bar{v}(p_1)(2\not{k}_3 - \not{p}_1 - \not{p}_2)[(\frac{1}{2} - s_w^2)P_L - s_w^2P_R]u(p_2) \\ &\quad \bar{u}(k_1, m_t) \left[m_b \tan \beta P_R + m_t \cot \beta P_L \right] v(k_2, m_b) \end{aligned}$$

$$\begin{aligned}
\mathcal{M}_{2d} &= \frac{-ig\mathcal{G}P^{\mu\nu\alpha\beta}}{16\sqrt{2}m_w[(k_1+k_3)^2-m_b^2]} \bar{v}(p_1)C_{\mu\nu}u(p_2) \\
&\quad \bar{u}(k_1, m_t) \left[m_b \tan \beta P_R + m_t \cot \beta P_L \right] (\not{k}_1 + \not{k}_3 + m_b) \chi_{\alpha\beta}^b v(k_2, m_b) \\
\mathcal{M}_{2e} &= \frac{ig\mathcal{G}P^{\mu\nu\alpha\beta}}{16\sqrt{2}m_w[(k_2+k_3)^2-m_t^2]} \bar{v}(p_1)C_{\mu\nu}u(p_2) \\
&\quad \bar{u}(k_1, m_t) \chi_{\alpha\beta}^c (\not{k}_2 + \not{k}_3 - m_t) \left[m_b \tan \beta P_R + m_t \cot \beta P_L \right] v(k_2, m_b) \\
\mathcal{M}_{2f} &= \frac{-ig\mathcal{G}P^{\mu\nu\alpha\beta}\chi_{\alpha\beta}^d}{4\sqrt{2}m_w[(k_1+k_2)^2-m_{H-}^2]} \bar{v}(p_1)C_{\mu\nu}u(p_2) \\
&\quad \bar{u}(k_1, m_t) \left[m_b \tan \beta P_R + m_t \cot \beta P_L \right] v(k_2, m_b) \\
\mathcal{M}_{2g} &= 0
\end{aligned} \tag{4}$$

with

$$\mathcal{G} = \frac{-1}{\bar{M}_p^2} \sum_{\vec{n}} \frac{1}{s - m_{\vec{n}}^2} \tag{5}$$

$$C_{\mu\nu} = [\gamma_\mu(p_2 - p_1)_\nu + (\mu \leftrightarrow \nu)] \tag{6}$$

$$\chi_{\alpha\beta}^a = m_{H-}^2 \eta_{\alpha\beta} - (k'_1)^\mu (k'_2)^\nu [\eta_{\mu\alpha} \eta_{\nu\beta} + \eta_{\nu\alpha} \eta_{\mu\beta} - \eta_{\mu\nu} \eta_{\alpha\beta}] \tag{7}$$

$$\chi_{\alpha\beta}^b = [\gamma_\alpha(k_1 + k_3 - k_2)_\beta - \eta_{\alpha\beta}(\not{k}_1 + \not{k}_3 - \not{k}_2 - 2m_b)] + (\beta \leftrightarrow \alpha) \tag{8}$$

$$\chi_{\alpha\beta}^c = [\gamma_\alpha(k_1 - k_3 - k_2)_\beta - \eta_{\alpha\beta}(\not{k}_1 - \not{k}_2 - \not{k}_3 - 2m_t)] + (\beta \leftrightarrow \alpha) \tag{9}$$

$$\chi_{\alpha\beta}^d = m_{H-}^2 \eta_{\alpha\beta} - k_3^\mu (k_1 + k_2)^\nu [\eta_{\mu\alpha} \eta_{\nu\beta} + \eta_{\nu\alpha} \eta_{\mu\beta} - \eta_{\mu\nu} \eta_{\alpha\beta}], \tag{10}$$

where $s \equiv (p_1 + p_2)^2$, $P_L = (1 - \gamma_5)/2$, $P_R = (1 + \gamma_5)/2$, $s_w = \sin_w$, $c_w = \cos_w$ and $\tan \beta$ is the ratio of the two vacuum expectation values in the 2HDM. Note that the contribution from Feynman diagram Fig.2(g) vanishes since the trace of the graviton appears in this diagram and, therefore, in the limit of vanishing electron mass, this contribution also vanishes[17].

\mathcal{G} in Eq. (5) represents the summation of the KK excitation propagators. If the summation over the infinite tower of the KK modes is performed, one will encounter ultraviolet divergences. This happens because LED is an effective theory, which is only valid below an effective energy scale. In the following calculations we naively introduce an ultraviolet cutoff for the highest KK modes and replace the summation by[15]

$$\frac{4\pi}{\Lambda_T^4} = \frac{-1}{\bar{M}_p^2} \sum_{\vec{n}} \frac{1}{s - m_{\vec{n}}^2}, \tag{11}$$

where Λ_T is a cutoff scale naturally being of the order of the fundamental scale M_s .

Finally, the cross sections for the charged Higgs production processes in LED following from the amplitudes are:

$$\sigma(e^+e^- \rightarrow H^+H^-) = \frac{1}{2s} \int d\Phi_2 \frac{1}{4} |M_{1a} + M_{1b}|^2 \quad (12)$$

$$\sigma(e^+e^- \rightarrow H^-t\bar{b}) = \frac{1}{2s} \int d\Phi_3 \frac{3}{4} |M_{2a} + M_{2b} + M_{2c} + M_{2d} + M_{2e} + M_{2f} + M_{2g}|^2, \quad (13)$$

and the final state phase space hypercube elements are defined as

$$d\Phi_2 = \left(\prod_{i=1}^2 \frac{d^3 \vec{k}'_i}{(2\pi)^3 2(k'_i)^0} \right) (2\pi)^4 \delta \left(p_1 + p_2 - \sum_{j=1}^2 k'_j \right). \quad (14)$$

$$d\Phi_3 = \left(\prod_{i=1}^3 \frac{d^3 \vec{k}_i}{(2\pi)^3 2k_i^0} \right) (2\pi)^4 \delta \left(p_1 + p_2 - \sum_{j=1}^3 k_j \right). \quad (15)$$

III. NUMERICAL RESULTS

In the numerical calculations, we used the following set of SM parameters[18]:

$$\alpha_{ew}(m_W) = 1/128, m_W = 80.419 \text{GeV}, m_t = 178 \text{GeV}, m_Z = 91.1882 \text{GeV}. \quad (16)$$

For the Yukawa coupling of the bottom quark at the $H^-t\bar{b}$ vertex, as suggested by Ref.[13], we used the top quark pole mass and the QCD improved running mass $m_b(Q)$ with $m_b(m_b) = 4.25 \text{ GeV}$, which were evaluated using the NLO formula [19] as follows:

$$m_b(Q) = U_6(Q, m_t) U_5(m_t, m_b) m_b(m_b), \quad (17)$$

Here the evolution factor U_f is

$$U_f(Q_2, Q_1) = \left(\frac{\alpha_s(Q_2)}{\alpha_s(Q_1)} \right)^{d(f)} \left[1 + \frac{\alpha_s(Q_1) - \alpha_s(Q_2)}{4\pi} J^{(f)} \right],$$

$$d(f) = \frac{12}{33 - 2f}, \quad J^{(f)} = -\frac{8982 - 504f + 40f^2}{3(33 - 2f)^2}, \quad (18)$$

and f is the number of active light quarks. For the energy scale Q , we chose $Q = \sqrt[3]{m_t m_b m_{H^-}}$ as in Ref. [13] for $e^+e^- \rightarrow H^-t\bar{b}$.

A. $e^+e^- \rightarrow H^+H^-$

In Fig. 3 we show the dependence of the the cross sections in 2HDM II and LED for the process $e^+e^- \rightarrow H^+H^-$ on m_{H^-} assuming $\sqrt{s} = 1000 \text{ GeV}$. The dashed lines represent

the 2HDM II results and the solid lines represent the cross section in 2HDM II LED for different values of Λ_T . From the figures one can see that when m_{H^-} is small(< 400 GeV) the LED effects can be very large up to $\Lambda_T = 2$ TeV. For example, when $\sqrt{s} = 1$ TeV and $m_{H^-} = 200$ GeV the cross section in the 2HDM is 23.8fb, while for 2HDM II LED it is 152.4fb for $\Lambda_T = 1.5$ TeV and 36.6fb for $\Lambda_T = 2$ TeV.

In Fig. 4, the cross section in the 2HDM II and LED for the process $e^+e^- \rightarrow H^+H^-$ are plotted as functions of \sqrt{s} assuming $m_{H^-} = 200$ GeV. From this figure we see that the effects of virtual graviton exchange can substantially modify the $e^+e^- \rightarrow H^+H^-$ cross section compared to its 2HDM II value, especially at large $\sqrt{s}(> 4$ TeV), enabling LED up to $\Lambda_T = 8$ TeV to be probed.

In Fig. 5 we show the dependence of the cross sections in the 2HDM II and LED for the process $e^+e^- \rightarrow H^+H^-$ on the effective energy scale Λ_T assuming $m_{H^-} = 150$ GeV and $\sqrt{s} = 1000$ GeV, 2000 GeV, and 3000 GeV. As expected, when \sqrt{s} is fixed the cross section in LED tends to the value in the 2HDM II when Λ_T tends becomes very large. In addition, the figure also shows that for large \sqrt{s} and small Λ_T the LED effects are very large. For example, for $\sqrt{s}=3$ TeV and $\Lambda_T=4$ TeV the cross section in the 2HDM II is 3.4fb while the value in LED is 58.7fb.

In Fig. 6, we present the differential cross section $d\sigma/d\cos\theta$ in the 2HDM II and LED for the process $e^+e^- \rightarrow H^+H^-$ as a function of $\cos\theta$, where the scattering angle θ is the angle between H^- and the incoming positron assuming $m_{H^-} = 200$ GeV, $\sqrt{s} = 1000$ GeV, and $\Lambda_T = 2000$ GeV. Both differential cross sections in the 2HDM II and LED vanish at $\cos\theta = \pm 1$. However, their shapes are different. Note that the LED cross section is not symmetric under $\cos\theta \leftrightarrow -\cos\theta$ while the 2HDM II one is symmetric. We further have plotted the different contributions to the LED cross section and find the asymmetry comes from the interference of the LED and 2HDM II amplitudes, which is in proportion to $(t - u)(tu - m_{H^-}^4)/\Lambda_T^2$ (t and u are Mandelstam variables) and thus to $\cos\theta \sin^2\theta$. Moreover, the LED contribution has peaks in both the forward and backward regions and also vanishes at three points: $\cos\theta = 0$ and ± 1 , as found in Ref. [20], since it is proportional to $(t - u)^2(tu - m_{H^-}^4)/\Lambda_T^4$ and thus to $\cos^2\theta \sin^2\theta$.

B. $e^+e^- \rightarrow H^-t\bar{b}$

In Fig. 7, we show the dependence of the the cross section in the 2HDM II and LED for the process $e^+e^- \rightarrow H^-t\bar{b}$ on m_{H^-} assuming $\sqrt{s} = 1000$ GeV for $\tan\beta = 40$. The dashed lines represent the 2HDM II results and the solid lines represent the cross sections for LED with different values of Λ_T . This figure shows that when Λ_T is small(< 2.5 TeV) and m_{H^-} is also small(< 600 GeV), the LED effects are very large. For example, when $\tan\beta = 40$ and $m_{H^-} = 550$ GeV the cross section in the 2HDM II is 0.017fb.

In Fig. 8, we present the dependence of the cross section in the 2HDM II and for LED for the process $e^+e^- \rightarrow H^-t\bar{b}$ on $\tan\beta$ assuming $\sqrt{s} = 1000$ GeV and $m_{H^-} = 520$ GeV. Observe that the cross section in both the 2HDM II and LED exhibit minima close to $\tan\beta \approx \sqrt{m_t/m_b} \approx 6$, since the average strength of the $t\bar{b}H^-$ coupling, which is proportional to $\sqrt{m_t^2 \cot^2 \beta + m_b^2 \tan^2 \beta}$, is then minimal [21]. From these figures one also sees that when $\Lambda_T = 2$ is small(< 2.5 TeV) and m_{H^-} is also small(< 600 GeV) the LED effects are large for $\sqrt{s} = 1$ TeV.

In Fig. 9 the cross sections in the 2HDM II and LED for the process $e^+e^- \rightarrow H^-t\bar{b}$ are plotted as functions of \sqrt{s} , assuming $m_{H^-} = 800$ GeV and $\tan\beta = 40$. Since we are interested in the case where $\sqrt{s}/2 < m_{H^\pm} < \sqrt{s} - m_t - m_b$, \sqrt{s} should be in the range from about 983 GeV to 1600 GeV. From this figure we see that, as in the case of $e^+e^- \rightarrow H^+H^-$, the effects of virtual graviton exchange can significantly modify the $e^+e^- \rightarrow H^-t\bar{b}$ cross section compared to its 2HDM II value, especially at large $\sqrt{s}(> 1.5$ TeV), where LED up to about $\Lambda_T = 3.5$ TeV can be probed.

In Fig. 10 we show the dependence of the cross section in the 2HDM II and LED for the process $e^+e^- \rightarrow H^-t\bar{b}$ on the effective energy scale Λ_T assuming $m_{H^-} = 260, 550, and 1100$ GeV, and $\sqrt{s} = 500, 1000$, and 2000 GeV, respectively. As expected, when \sqrt{s} is fixed the LED cross section tends to the value in the 2HDM II when Λ_T becomes very large. This figure also shows that for large \sqrt{s} and small Λ_T the LED effects can be very large. For example, when $\sqrt{s}=2$ TeV and $\Lambda_T=4$ TeV the cross section in the 2HDM II is 0.006fb, while in LED it is 0.013fb.

In Fig. 11 we show the differential cross sections $d\sigma/dP_T(H^-)$ in the 2HDM II and LED for the process $e^+e^- \rightarrow H^-t\bar{b}$ as functions of the transverse momentum of the charged Higgs boson P_T assuming $m_{H^-} = 520$ GeV, $\sqrt{s} = 1000$ GeV, and $\Lambda_T = 1500$ GeV, 2000 GeV,

2500 GeV and 3000 GeV. The shape of the differential cross sections in the 2HDM II and for LED are slightly different. The LED effects generally enhance the differential cross sections, especially when Λ_T is small.

We briefly note the relevant results in type I 2HDM. The only change is in the fermionic couplings. Thus, the 2HDM and LED results for $e^+e^- \rightarrow H^+H^-$ remain the same. However, the 2HDM results for $e^+e^- \rightarrow H^-t\bar{b}$ in the type I model are different compared with the type II model. For example, the results in type I model will decrease with increasing $\tan\beta$, since the $H^-t\bar{b}$ coupling is proportional to $\cot\beta$ in the type I model. However, the LED effects will be similar: large effects when \sqrt{s} is large and Λ_T is small.

Finally, we briefly discuss the experimental sensitivity. We will assume that the LED effects can be observed, if[22]

$$\Delta\sigma = \sigma_{LED} - \sigma_{SM} \geq \frac{5\sqrt{\sigma_{LED}\mathcal{L}}}{\mathcal{L}}, \quad (19)$$

where the integrated luminosity \mathcal{L} are assumed to be 500fb^{-1} . For $e^+e^- \rightarrow H^+H^-$, from Fig. 5, we see that the LED can be probed, for example, up to 2800 GeV and 7200 GeV with $m_{H^-} = 150$ GeV for $\sqrt{s} = 1000$ GeV and 3000 GeV, respectively. For $e^+e^- \rightarrow H^-t\bar{b}$, from Fig. 10, we see that the LED can be probed, for example, up to 1400 GeV and 3600 GeV for $m_{H^-} = 260$ and 1100 GeV, and $\sqrt{s} = 500$, and 2000 GeV, respectively.

IV. SUMMARY

In the 2HDM II with large extra dimensions we investigated the contributions of virtual KK gravitons for the 2HDM II charged Higgs production in the two important production processes: $e^+e^- \rightarrow H^+H^-$ and $e^+e^- \rightarrow H^-t\bar{b}$ at future linear colliders. We found that KK gravitons can significantly modify these total cross sections and their differential cross sections compared to the corresponding 2HDM II values and, therefore, can be used to probe the effective scale Λ_T up to several TeV. For example, at $\sqrt{s} = 2$ TeV the cross sections for $e^+e^- \rightarrow H^+H^-$ and $e^+e^- \rightarrow H^-t\bar{b}$ in the 2HDM II are 7.4 fb for $m_{H^-} = 150$ GeV and 0.006 fb for $m_{H^-} = 1.1$ TeV with $\tan\beta = 40$, while in LED they are 12.1 fb and 0.013 fb, respectively, for $\Lambda_T = 4$ TeV.

Acknowledgments

We thank Prasanta Kumar Das for useful discussions. This work was supported in part by the National Natural Science Foundation of China, under grant Nos.10421003 and 10575001, and the Key Grant Project of Chinese Ministry of Education, under grant NO.305001, and the U.S. Department of Energy, Division of High Energy Physics, under Grant No.DE-FG02-91-ER4086.

- [1] N. Arkani-Hamed et al., *Phys.Lett.* B429 (1998) 263; N. Arkani-Hamed et al., *Phys.ReV.* D59 (1999) 086004; N. Arkani-Hamed et al., *Phys.Lett.* B436 (1998) 257.
- [2] L. Randall, R.Sundrum, *Phys.Rev.Lett.* 83 (1999) 3370; L. Randall, R.Sundrum, *Phys.Rev.Lett.* 83 (1999) 4690.
- [3] J. Lykken, *Phys.ReV.* D54 (1996) 3693.
- [4] E. Witten, *Nucl.Phys.* B471 (1996) 135.
- [5] P. Horava and E. Witten, *Nucl.Phys.* B460 (1996) 506; *Nucl.Phys.* B475 (1996) 94.
- [6] I. Antoniadis, *Phys.Lett.* B246 (1990) 377.
- [7] S. Glashow and S. Weinberg, *Phys.Rev.* D15 (1977) 1958; J. F. Gunion et. al., 1990, Higgs Hunter's Guide(Reading, MA: Addison-wesley).
- [8] C. Csaki, TASI Lectures on Extra Dimensions and Branes, [hep-ph/0404096](#).
- [9] E. G. Adelberger [Eot-Wash Group Collaboration] [hep-ex/0202008](#).
- [10] T. Hambye and K. Riesselmann, *Phys.Rev.* D55 (1997) 7255.
- [11] S. Komamiya, *Phys.Rev.* D38 (1988) 2158; J. Guasch et al., *Nucl.Phys.* B596 (2001) 66.
- [12] S. Kanemura et al., *JHEP* 0102 (2001) 011; A. Djouadi et al., *Z. Phys.* C54 (1992) 255
- [13] B. A. Kniehl et al., *Phys.Rev.* D66 (2002) 054016.
- [14] H. E. Haber and G. L. Kane, *Phys.Rep.* 117 (1985) 75.
- [15] G. F. Giudice et al., *Nucl.Phys.* B544 (1999) 3.
- [16] T. Han, J. D. Lykken and R. J. Zhang, *Phys.Rev.* D59 (1999) 105006.
- [17] D. Choudhury, N. G. Deshpande, D. K. Ghosh, *JHEP* 0409 (2004) 055.
- [18] Particle Data Group, S. Eidelman, et al., *Phys. Lett.* B592 (2004) 1.
- [19] M. Carena et al., *Nucl.Phys.* B577 (2000) 88.

- [20] N. Delerue et al., Phys.Rev.D70 (2000) 091701.
- [21] A. Krause et al., Nucl.Phys.B519 (1998) 85.
- [22] S. Hao et. al., Phys.Rev.D71 (2005) 075005.

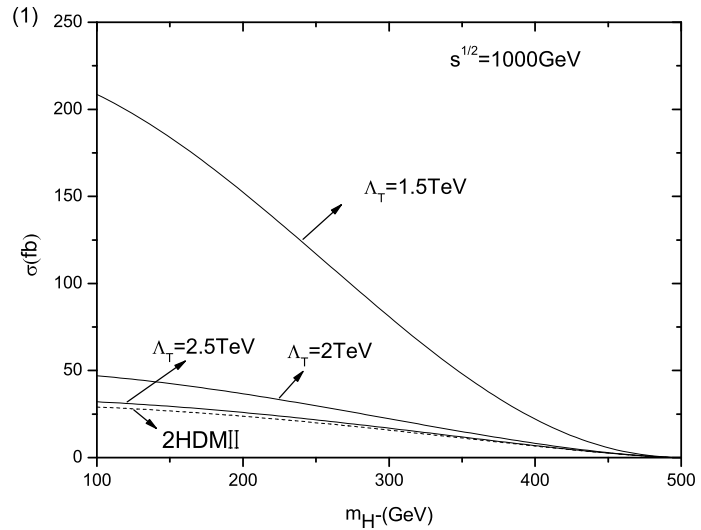


FIG. 3: Dependence of the cross section in the 2HDM II and LED for the process $e^+e^- \rightarrow H^+H^-$ on m_{H^-} , assuming $\sqrt{s} = 1000 \text{ GeV}$.

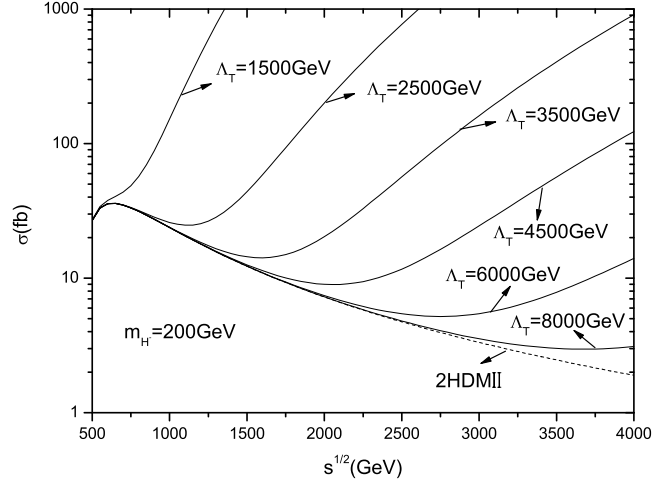


FIG. 4: Dependence of the cross section in the 2HDM II and LED for the process $e^+e^- \rightarrow H^+H^-$ on \sqrt{s} , assuming $m_{H^-} = 200$ GeV.

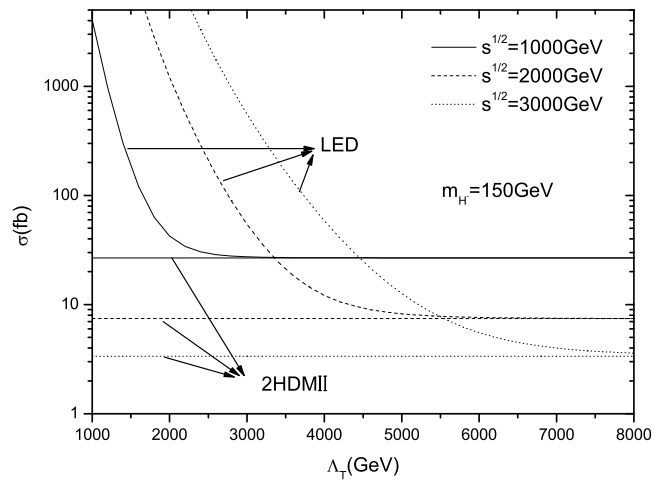


FIG. 5: Dependence of the cross section in the 2HDM II and LED for the process $e^+e^- \rightarrow H^+H^-$ on the effective energy scale Λ_T , assuming $m_{H^-} = 150$ GeV, $\sqrt{s} = 1000$ GeV, 2000 GeV, and 3000 GeV.

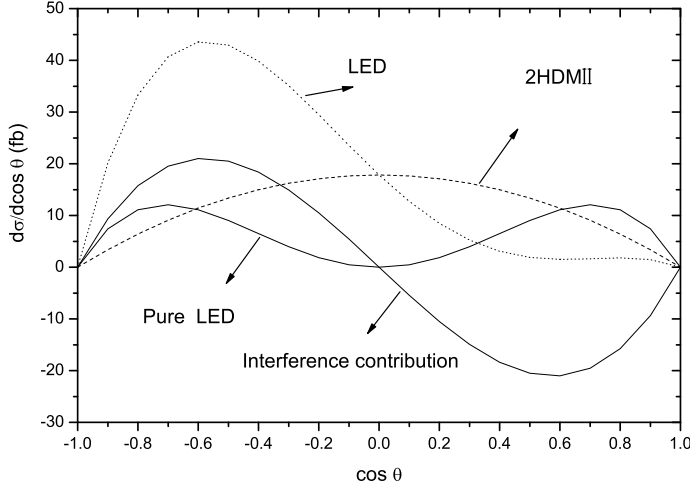


FIG. 6: The differential cross section $d\sigma/d\cos\theta$ in the 2HDM II and LED for the process $e^+e^- \rightarrow H^+H^-$ as functions of $\cos\theta$, assuming $m_{H^-} = 200$ GeV, $\sqrt{s} = 1000$ GeV, $\Lambda_T = 2000$ GeV.

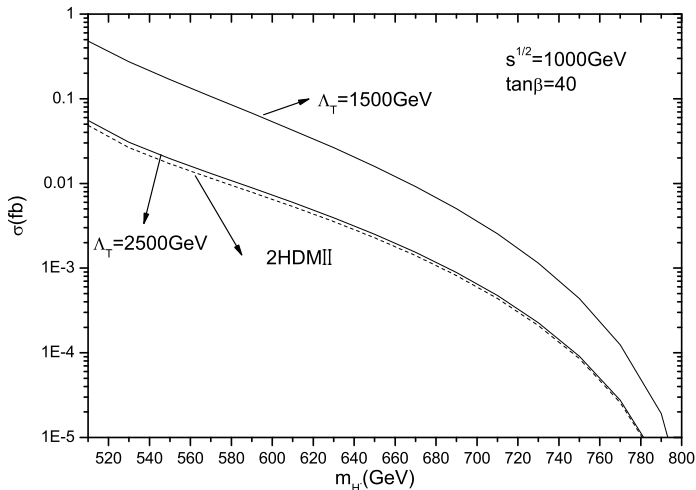


FIG. 7: Dependence of the cross section in the 2HDM II and LED for the process $e^+e^- \rightarrow H^-t\bar{b}$ on m_{H^-} , assuming $\sqrt{s} = 1000$ GeV, $\tan\beta = 40$.

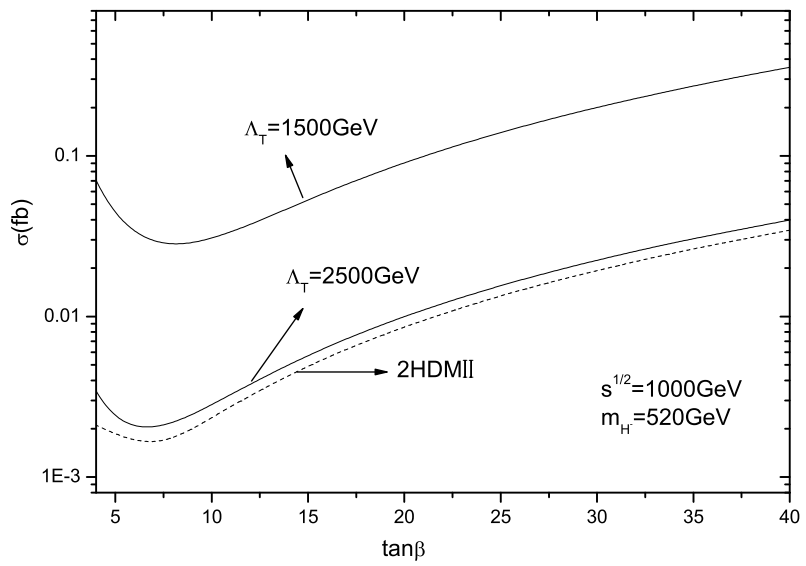


FIG. 8: Dependence of the cross section in the 2HDM II and LED for the process $e^+e^- \rightarrow H^-t\bar{b}$ on $\tan\beta$, assuming $\sqrt{s} = 1000$ GeV, $m_{H^-} = 520$ GeV.

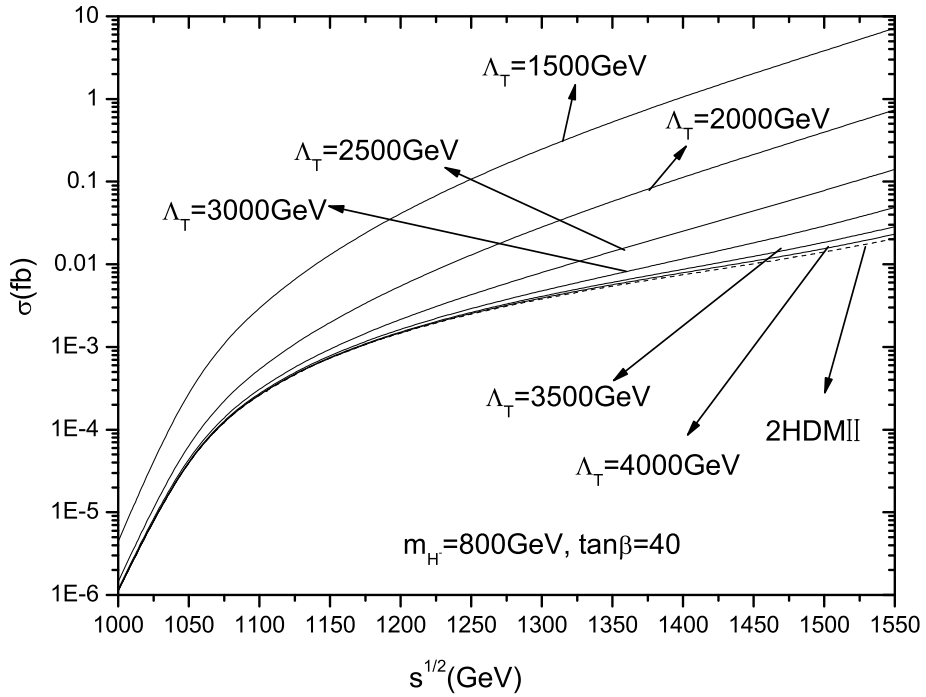


FIG. 9: Dependence of the cross section in the 2HDM II and LED for the process $e^+e^- \rightarrow H^-t\bar{b}$ on \sqrt{s} , assuming $m_{H^-} = 800$ GeV, $\tan \beta = 40$.

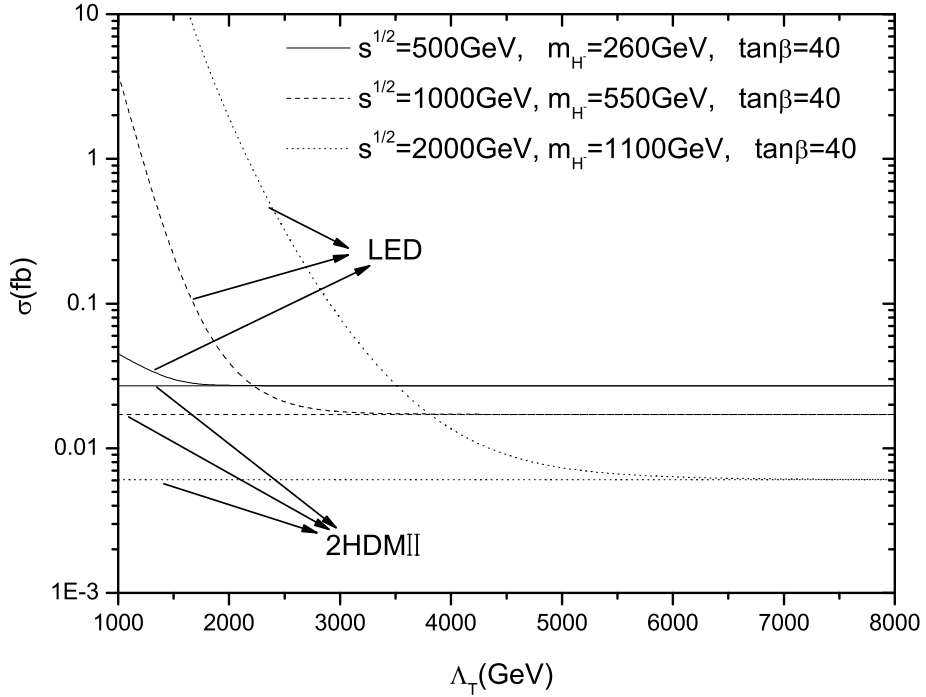


FIG. 10: Dependence of the cross section in the 2HDM II and LED for the process $e^+e^- \rightarrow H^-t\bar{b}$ on the effective energy scale Λ_T , assuming $m_{H^-} = 260, 550, 1100$ GeV, and $\sqrt{s} = 500, 1000, 2000$ GeV, respectively.

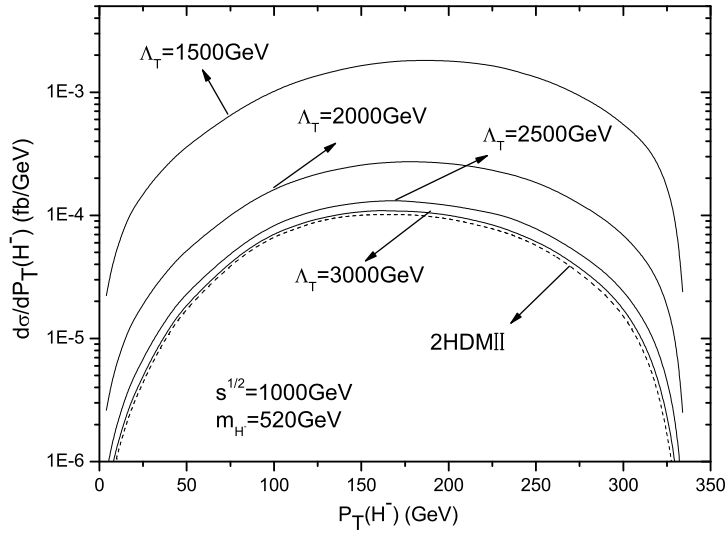


FIG. 11: The differential cross section $d\sigma/dP_T(H^-)$ in the 2HDM II and LED for the process $e^+e^- \rightarrow H^-t\bar{b}$ as a function of the transverse momentum of the charged Higgs boson P_T , assuming $m_{H^-} = 520$ GeV, $\sqrt{s} = 1000$ GeV, $\Lambda_T = 1500$ GeV, 2000 GeV, 2500 GeV and 3000 GeV.